Environmental Earth Sciences (2025) 84:7
https://doi.org/10.1007/s12665-024-12009-y

ORIGINAL ARTICLE

Integrated geological study in an offshore renewable energy test site: a case from the Basque continental shelf (Bay of Biscay, Spain)

Iván Asensio[1] · Lidia Rodríguez-Méndez[2] · Néstor Vegas[2] · Aitor Aranguren[2]

Received: 30 July 2024 / Accepted: 30 November 2024

Abstract

Testing and research centres for offshore renewable energy, exemplified by facilities like BIMEP (Biscay Marine Energy Platform) on the Basque coast of Spain, play a crucial role in driving the energy transition. This study utilises pre-existing data at the facility site, such as high-resolution bathymetry and granulometric information from sediment samples, to conduct a comprehensive geological analysis including both sedimentary and rocky seabed. A litho-structural analysis is presented, including a lithological prediction for the continental shelf, the recognition of the main structures, such as NW-trending folds and predominantly NE-SW oriented fractures, and a detailed fracture analysis. Sedimentary seabeds are analysed through a Seabed Sediment Map, illustrating a granulometry-based NE-SW oriented banded distribution. Bedforms are also studied, they are asymmetric and mainly oriented NE-SW. The Seabed Sediment Map and the bedform analysis reveal the effect of an SE-directed bottom current as the main mechanism controlling sediment mobility. This current matches with the predominant swell from the NW and with the direction of the most energetic waves in the area. This approach could serve as a methodological example, offering a cost-effective means for the preliminary geological characterisation of offshore energy sites, and is crucial for establishing a baseline ('zero state') before the deployment. This baseline is essential for evaluating and mitigating the impact of new infrastructure on sediment dynamics, which subsequently affects the overall functioning and health of the marine ecosystem.

Keywords Marine energy · Basque-Cantabrian Basin · Sediment mapping · Fracture analysis · Bay of Biscay · BIMEP

Introduction

Renewable energies play a crucial role in mitigating climate change by offering sustainable alternatives to fossil fuels. To keep global warming under 1.5 ºC, compared to the 2010 level, emissions need to be reduced by 45% by 2030 and reach net-zero by 2050 (United-Nations 2015). A growing coalition of countries, including the biggest polluters (the European Union, the United States, India and China), have set a net-zero target (Net-Zero-Tracker 2023), signalling a significant shift towards environmental sustainability on a global scale. The development of offshore renewable energies is fundamental for addressing the challenges of climate change, greenhouse gas emission reduction, energy security and economic development. The European Net Zero Industry Act (2023) emphasises marine renewable energies as one of the key strategic technologies that could make a significant contribution to decarbonisation by 2030.

In this scenario, the trend in the offshore wind market is steadily growing, and with it, the need to install more farms and adapt the deployment of the devices to the specific characteristics of installation sites (Jiang 2021; Quero García et al. 2020; Vázquez et al. 2024). A crucial aspect in the development of offshore wind farms is installation and maintenance costs, which are strongly conditioned by the geological characteristics of the sites (Petrie Hannah

✉ Lidia Rodríguez-Méndez
lidia.rodriguez@ehu.eus

Iván Asensio
asensio.cantero@gmail.com

Néstor Vegas
nestor.vegas@ehu.eus

Aitor Aranguren
aitor.aranguren@ehu.eus

[1] Irun, Spain

[2] Departamento de Geología, Facultad de Ciencia y Tecnología, Universidad del País Vasco/Euskal Herriko Univertsitatea UPV/EHU, Barrio Sarriena S/N, 48940 Leioa, Spain

Published online: 11 December 2024

et al. 2022). As optimising these operations is necessary to reduce the final price of energy and improve project profitability, it becomes increasingly important to understand the sub-surface structure and the seabed configuration at offshore energy sites (Velenturf et al. 2021). For instance, understanding the general geological structure, such as sedimentary vs. rocky seabed distribution, sediment thickness, and depth to bedrock, is essential for engineering considerations. Insights into fracture patterns are also crucial for evaluating the stability of structures installed on the seabed, like monopiles or other fixed foundations. These factors are particularly important during the planning and projecting phase of offshore infrastructures.

Moreover, sediments play a crucial role in nutrient dynamics, turbidity, and light attenuation, thereby significantly impacting the overall health and functioning of the ecosystem (Clark et al. 2014). Understanding sediment characteristics is essential as they can serve as sinks for various types of pollutants, thus affecting water quality and the overall stability of aquatic environments (Wang et al. 2023). Specifically, comprehending sediment mobility is vital for predicting sediment transport patterns and their interaction with offshore installations in order to mitigate their potential impact on both the devices and the habitat (Amjadian et al. 2023; Cai et al. 2023; Galparsoro et al. 2022; Velenturf et al. 2021).

Conducting observational studies before, during and after construction is necessary to gain this understanding, establish a baseline (undisturbed state) for comparing subsequent changes, and ensure an accurate assessment of the project´s impact on the environment. Bathymetric, geophysical, and geotechnical studies conducted according to each country´s specifications for installing marine renewable energy farms provide relevant geological information. Although these datasets may sometimes be incomplete, they can still offer valuable insights for general geological characterisation when properly extracted, processed, and analysed. Effectively utilising this initial data during the engineering projection phase, as well as in later stages of exploration and development, allows for a more efficient resource allocation, ensuring a focused and streamlined approach.

This study aims to perform an integrated analysis of the main geological features of BIMEP (Biscay Marine Energy Platform), a test site located on the Spanish coast of the Bay of Biscay (Fig. 1A). Operational since 2015, BIMEP is an open-sea testing facility for ocean energy collectors and auxiliary equipment. Among the devices tested and installed in BIMEP are DemoSATH (https://saitec-offshore.com/es/projects/demosath/), a full-scale prototype of a 2 MW wind turbine, and HarshLab (https://harshlab.eu/), a floating laboratory to test materials and components in marine environments. In addition to offering a designated marine area restricted to shipping, BIMEP provides researchers and companies with the main technical characteristics of the test field, as well as information on the bathymetry and hydrodynamic conditions. This work utilises pre-existing data from BIMEP to conduct a comprehensive geological study that includes both sedimentary and rocky seabed and could serve as a methodological example that offers a cost-effective means to perform a preliminary geological characterisation of offshore energy sites. The approach integrates various data sources in order to conduct a lithological study, fracture analysis, seabed mapping and sediment mobility analysis through the study of bedforms. The obtained results provide valuable information to optimise the installation and maintenance processes of devices and infrastructures located on the continental shelf, thereby contributing to cost reduction and increased competitiveness in the renewable energy sector. Furthermore, it enhances regional geological knowledge, which is crucial for environmental protection plans, coastal risk assessment, and in general, for planning coastal development and any other offshore infrastructure.

Geological and oceanographic setting

Regional geology

The study area is situated in southwestern Europe, in the northern part of the Iberian Peninsula, and comprises a sector of the Basque coastline and the adjacent continental shelf up to 96 m in depth, close to the locality of Armintza (Fig. 1A, B). From a geological perspective, this study falls within the Basque-Cantabrian Basin (BCB), an example of a hyperextended rift that underwent inversion during the Alpine Orogeny and represents the western prolongation of the Pyrenean chain. Extensional tectonics occurred during the Permian–Triassic and the Jurassic-Lower Cretaceous periods (Tugend et al. 2014). During Albian times, extreme stretching and crustal thinning took place, leading to the exhumation of lithosphere (Pedrera et al. 2021) coeval with marine sedimentation (Lagabrielle and Bodinier 2008; Tugend et al. 2014) and alkaline magmatism up to the Santonian (Lamolda et al. 1983; Ubide et al. 2014). The BCB, particularly in the northern sector where this study is located (Basque Arc), exhibits a complex structure due to the onset of compressive tectonics initiated during the Campanian period (Gómez et al. 2002) over a continental crust previously deformed under extensional tectonics (DeFelipe et al. 2018; Pedreira et al. 2007). At the regional level, the study area is situated on the northeastern limb of the Biscay Synclinorium, an asymmetric structure characterised by a NW–SE orientation and north-eastward vergence, that can be identified over 90 km onshore and an additional 13 km offshore (Rodríguez-Méndez et al. 2022).

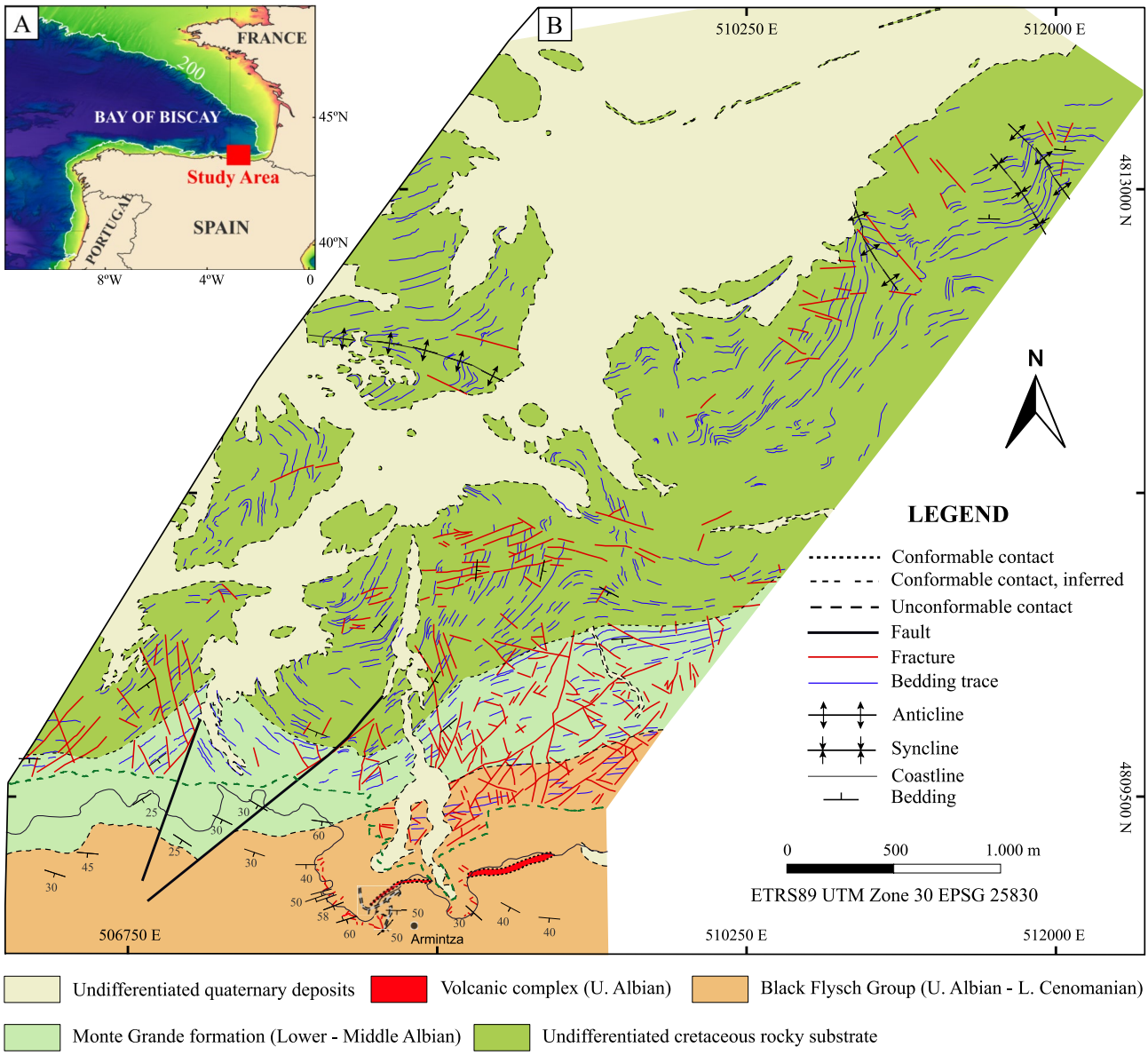

Fig. 1 **a** Location of the study area in the north of Spain, on the Basque coast; **b** Geological map up to 96 m depth, including bedding traces and fracture network cartography (modified from Asensio et al. (2024)). The green dashed line represents the extent of the multibeam dataset

In close proximity to the study area, other notable structures include the Bakio diapir (Poprawski et al. 2014; Roca et al. 2021) and the Gorliz syncline.

Sedimentary and subvolcanic rock formations

A Cretaceous succession of sedimentary rocks (Albian-Cenomanian) with minor subvolcanic rocks interlayered covers the studied area. It shows a remarkable internal complexity with important geographical variations (Ábalos and Elorza 2012; Puelles et al. 2017). The oldest deposits in the area constitute the so-called Monte Grande formation (Lower-Middle Albian), a fan delta system deposited under overall marine transgression conditions (Robles et al. 1988), that rests on strongly karstified Lower Albian carbonates (out of the study area). It is composed of sandstones, silica-rich conglomerates and sandy mudstones rich in vegetable fragments (Asensio et al. 2024). Albian-Lower Cenomanian Black Flysch Group unconformably overlie the Monte Grande formation (Agirrezabala et al. 2023; Rat and Feuillée 1967) (Fig. 1B). The Black Flysch succession is deposited under deep marine environments and is divided into two depositional sequences (Robles et al. 1988). Submarine volcaniclastic rocks, basaltic pillow lavas and hyaloclastites of Upper Albian age (Castañares et al. 2001; Lopez-Horgue et al. 2009), regionally known as the Volcanic Complex, are

intercalated between the two sequences. López-Horgue et al. (2009) assigned an Early to Middle Albian age (histeroceras variscosum zone) to the lower sequence, formed by collapsing slope and resedimented coarse turbidites, with quartz-tectonite conglomerate and metasandstone pebbles that encapsulate evidence of pre-Mesozoic igneous and metamorphic events (Puelles et al. 2014). The Upper Sequence shows a Late Albian age (López-Horgue and Owen 2024; Lopez-Horgue et al. 2009) (inflatum zone) and is composed of a prograding slope of fine turbiditic systems with intercalated thin tuffs and various slumps (Ábalos and Elorza 2012).

Physiography

The continental shelf in this sector of the Bay of Biscay is characterised by its narrowness (7–20 km) (Uriarte 1998). It shows a staircase morphology, with 12 submerged terraces irregularly preserved, that is controlled by an interplay of variables such as wave climatology, lithology and bedding direction (Bilbao-Lasa et al. 2020). The outer shelf (down to 180 m water depth) is characterised by an almost flat surface that displays an intensively eroded seafloor surface (Ercilla et al. 2008). Referring to sediment supply along the Basque continental shelf, the major suppliers are coastal erosion and rivers, with an estimated $1.57{\cdot}10^{6}$ $t{\cdot}yr^{-1}$ of suspended material discharged by 12 main rivers (Ferrer et al. 2009; Uriarte et al. 2004). Low-salinity waters associated with river discharges are observed up to 50 m depth (Ferrer et al. 2009). The margin is considered starved due to the great sediment evacuation from the continental shelf to the slope (Ercilla et al. 2008). Previous works have provided a general overview of sediment distribution on the continental shelf (Galparsoro et al. 2010; Jouanneau et al. 2008), and more recently, Irabien et al. (2020) conducted a study on the anthropogenic impact on sedimentary beds off the coast of Gipuzkoa.

Oceanography

The southern part of the continental shelf of the Bay of Biscay is exposed to a large range of possible sea states, particularly in terms of wave height and period; as such, it is considered a high-energy environment (Iglesias and Carballo 2010). Particularly, the Basque coast faces significant exposure to large fetches due to its orientation and location relative to low-pressure systems forming in the North Atlantic (González et al. 2004). These storms generate strong winds and large waves predominantly from the northwest quadrant (Ibarra-Berastegi et al. 2018; OSPAR Commission 2000). Remarkably, the associated waves generate swell that persists even during periods of calm weather or with strong and relatively persistent winds from various directions, illustrating the enduring impact of the storms (Fontán et al. 2006; Galparsoro et al. 2010, 2012; Uriarte et al. 2004).

The circulation of water on the Basque shelf is primarily conditioned by the wind regime (Fontán and Cornuelle 2015; Fontán et al. 2009; González et al. 2006; Uriarte et al. 2004), except in estuaries, where the contribution of tides is also an important factor (González et al. 2004; Uriarte et al. 2004). The wind regime on the Basque coast has a seasonal component: in autumn–winter, winds mainly blow from the SW, producing currents towards the E and N; in spring, the wind comes from the NW, generating currents towards the W-SW. In summer, the situation is similar to that of spring but with less intense winds and more variable directions, resulting in weaker and less constant currents (González et al. 2004). The wind-generated surface currents have an average E-W orientation (Chiri et al. 2019; Ibañez 1979) that causes a coast-parallel transport of fine-grained sediments and pollutants (González et al. 2006; Uriarte et al. 2004).

Methods and data

This work is approached from an interdisciplinary perspective, integrating traditional geological techniques with an analysis based on indirect methods using the software QGIS. To perform the geological characterisation of the continental shelf, a combination of methods is employed:

1.- Lithological study and fracture analysis: a field study was conducted on the cliffs and the intertidal zone of Armintza to characterise the main lithologies and structures present at a scale of 1:2.500 using high-resolution orthophotos and a digital elevation model obtained from the Basque Government´s spatial data infrastructure (GeoEuskadi). In addition, bathymetric data provided by BIMEP were analysed. These data correspond to the campaign conducted by AZTI in 2017 (Bald 2017), for which a SeaBat 7125 multibeam echosounder was used. This echosounder consists of 256 beams within an angular sector of 130° and operated at a frequency of 400 kHz, installed on the vessel "Aztimar Bat". The echosounder has a vertical resolution of 6 mm and a maximum operating depth of 100 m. The bathymetric digital model resolution corresponds to a grid of 1×1 m^2, the finest resolution achievable with this equipment. QGIS was used to create hillshade, slope and roughness maps of the study area, covering depths from 2 to 96 m. A detailed analysis of the hillshade allowed the drawing of bedding traces and fractures, as well as establishing the main structures of the area. Using the geological map of the onshore zone at a scale of 1:25.000 (Garrote Ruiz et al. 1987) and the obtained geological data, the main lithological units and structures

were extended towards the shelf and a fracture analysis was conducted. The NetworkGT plugin for QGIS (Nyberg et al. 2018) was employed to extract the direction and length data of fractures, enabling a comprehensive fracture analysis.

2.- Seabed Sediment Map: A visual classification of three seabed types -unconsolidated sediment covered bottoms, rocky bottoms, and mixed bottoms- was conducted using the hillshade map as the primary reference, and slope and roughness maps as supplementary data. The hillshade map offered a high-resolution representation of the seafloor´s morphology, and the slope and roughness maps added critical details to refine the interpretation. In the case of mixed seabeds, the visual analysis identified areas where a thin layer of sediments is deposited, but lacked sufficient thickness to fully mask the topography of the underlying rocky substrate, which remained evident in the seafloor morphology. Following this, the granulometric analysis of 28 marine sediment samples conducted by Robotiker (2009) for BIMEP was utilized and the samples were reclassified into 4 categories, following the Folk (1954) sediment classification. Based on the distribution of the reclassified samples, Surfer software was used to perform an ordinary Kriging to create two maps: one providing an approximate distribution of the average sediment size, an another showing an approximate distribution of the gravel percentage (Seabed Sediment Map) based on the Folk (1954) classification.

Results and discussion

Lithological study

This study presents a continuous lithological analysis, covering a total area of about 19 km^2, from the continental zone to a depth of 96 m below the sea (Fig. 1). The lithological formations defined in the onshore regional cartography at 1:25.000 scale (Garrote Ruiz et al. 1987) were adopted, except for the distinctions within the Black Flysch group because they are not identifiable from the bathymetry. In general, the sedimentary succession shows dip directions towards the SW or SE, so increasingly older formations crop out towards the continental shelf. To establish the contact between the Monte Grande formation and the Black Flysch, fieldwork data, data obtained through the analysis of the hillshade, and previous studies (Asensio et al. 2024; Garrote Ruiz et al. 1987; Puelles et al. 2014; Robles et al. 1988) were considered. The lower portion of the Monte Grande formation is only occasionally observed to the west of the study area, where it rests on strongly karstified Lower Albian carbonates. In that area, the basal contact of the Monte Grande formation constitutes an unconformity deformed by a N-S trending fault with associated diatremes (Agirrezabala et al. 2017). In the study area, the contact between the basal part of the Monte Grande formation and the older Cretaceous succession is not exposed onshore. Considering that previous studies estimated a minimum thickness of 500 m for the Monte Grande formation (Pujalte et al. 1986), along with the available dip values and the identified faults, a tentative contact is represented in Fig. 1 to provide an approximate location. The rocks stratigraphically underneath the Monte Grande formation are represented as an undifferentiated rocky substrate of Lower Cretaceous age due to the lack of data for a more precise characterization. However, the examination of the hillshade map reveals an area north of the Monte Grande formation with well-defined bedding, suggesting a multi-layer sequence and discarding a massive limestone exposure. Complementary data, such as well data or seismic profiles, would be essential to precisely determine the lithology and the position of the contact.

Taking into account the hillshade analysis and bedding traces, folds, faults and fractures were identified. Folds are mainly located in the northernmost part of the study area and they display an orientation that ranges from NW–SE to WNW-ESE (Fig. 1B), coincident with the regional trend. When addressing brittle deformation, identifying kinematic criteria represents a significant challenge due to the very limited information about the faults provided by a low-relief area, like the continental shelf, where only a top-down perspective is available. Consequently, only two faults are identified in the southeastern part of the study area, exhibiting orientations ranging from NNE-SSW to NE-SW. They deform the contact between the Black Flysch group and the Monte Grande formation and induced an orientation change in the bedding trace that can be recognized in the bathymetry (Fig. 1B).

Fracture analysis

Through the hillshade and detailed orthophotograph analysis the main fractures of the study area were mapped. A total of 470 fractures were mapped, with a combined length of 49.6 km (Fig. 2).

For a more comprehensive statistical analysis, fractures have been depicted on a rose diagram with 10º intervals (Fig. 2A). The diagram reveals that the prevailing direction of fractures is concentrated between 40º and 60º (90 fractures). Additionally, two other preferred orientations can be identified: between 100 and 130º (107 fractures) and between 150 and 160º (63 fractures). When considering the length of each mapped fracture as a weighting factor, the resulting rose diagram exhibits some differences (Fig. 2B): the peak remains between 40 and 60º (8.3 km of cumulative length), and two other preferred directions emerge between 140 and 170º (7.98 km) and between 100 and 130º (7.65 km). In the weighted diagram, approximately the same preferred orientations as in the rose diagram are observed, but with

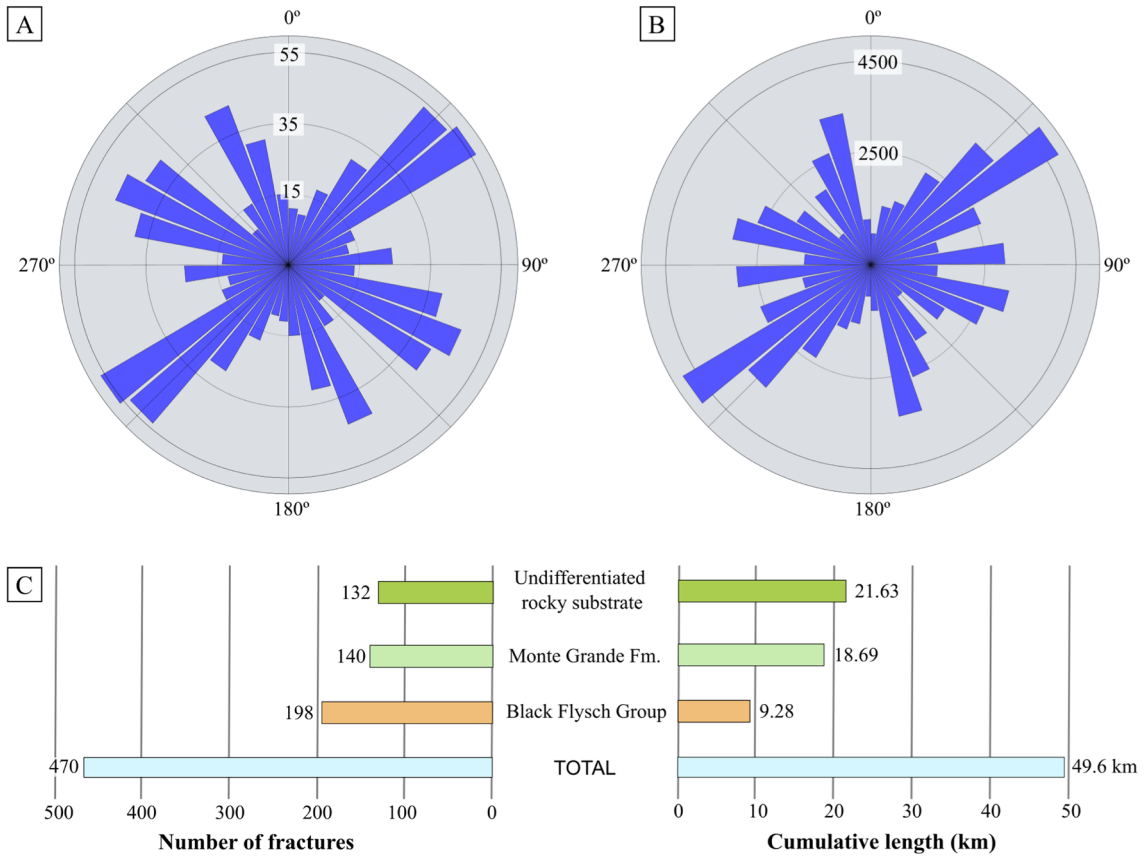

Fig. 2 **a** Equal area rose diagram with 10º bin width showing the distribution of the number of fractures according to their orientation; **b** Length (m) weighted equal area rose diagram with 10º bin; **c** Visual comparison of the fracture analysis based on the formation in which fractures appear. On the left, a representation of the number of fractures; on the right, the cumulative length

the difference that they all appear with similar importance. The results align with fracturing data from nearby sectors. The 100–130º fracture family corresponds with the main orientation of the cartographic-scale structures in this sector of the Basque Arc (Ábalos 2016), indicating the influence of regional tectonic features. Additionally, the 40–60º set coincides with the direction of a local kilometer-scale fault west of the study area (Garrote et al. 1987).

Taking into account the formation where the fractures occur (Fig. 2C), it is noted that the majority of fractures are located within the Black Flysch group (42%). However, when considering the cumulative length, the highest values correspond to the undifferentiated rocky substrate (21.63 km, 43.35%), followed by the Monte Grande formation (18.69 km, 37.45%).

Fracture analysis, such as that conducted at BIMEP, can identify potential risks like weak zones, enabling more informed decision-making and efficient planning of subsequent studies. Addressing these factors early ensures long-term stability and reduces the risk of costly delays, leading to safer and more cost-effective projects.

Seabed sediment map

Using a hillshade map generated from bathymetric data, the seabed across the study area (16.3 km^2) was mapped and categorized it into three types: rocky, sedimentary, and mixed (Fig. 3A). Our analysis reveals that 57.4% (9.35 km^2) of the studied area is composed of rocks, 38.5% (6.28 km^2) of sediments, and 4% (0.67 km^2) of mixed substrate. Rocky substrate predominate in the southern and eastern regions of the study area, while sedimentary substrate is more prevalent towards the north, although the presence of sediments along the channel in the southern zone is notable (Fig. 3A). Mixed seabed is confined to specific areas, typically occurring at the interface between sedimentary and rocky substrate or within rocky bottoms.

In order to obtain more information about sediment-covered bottoms, granulometric data derived from 28 samples performed by Robotiker (2009) for BIMEP was analysed and reinterpreted (see Fig. 3A to locate the samples). They show a mean grain size between 171–2535 µm, with sorting values between 0.4 and 1.7 phi and have an average organic matter content of 1.7% (Max.

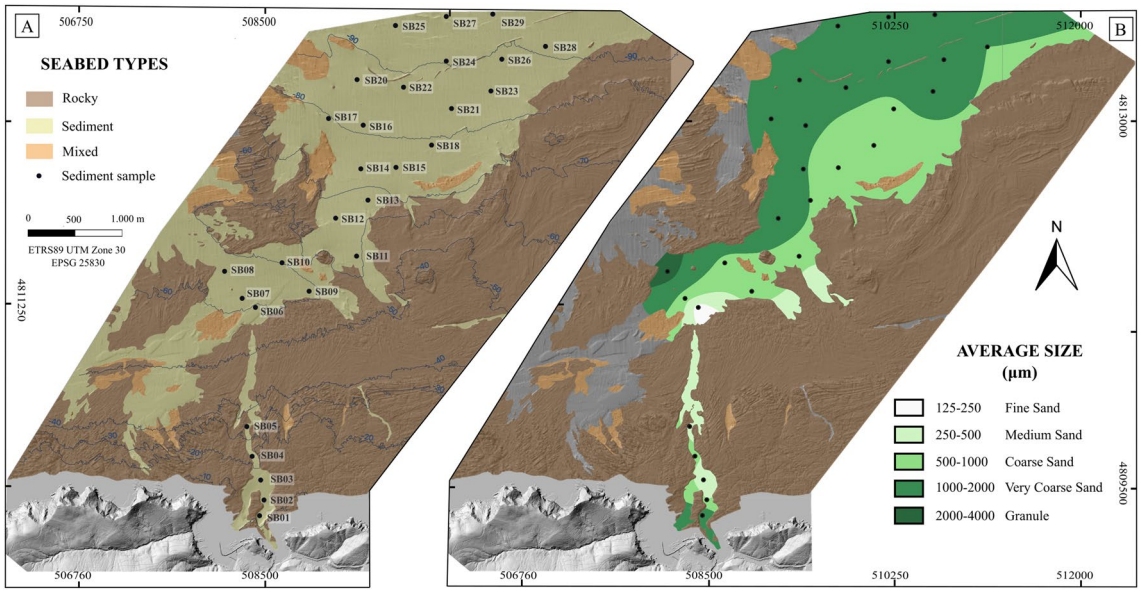

Fig. 3 **a** Seabed type map of the studied area with the location of the sediment samples. Isobaths at 10 m intervals are included; **b** Map of the Average size of the sediment (μm) according to Wentworth (1922) grain size classification

3.5%). Coarse grains predominate and only two samples display more than 1% of silt and clay (Table 1: SB6-2.57% and SB25-1.08%). An ordinary kriging interpolation, constrained to the area with available sediment sampling points, was employed to visualize the approximate distribution of the average sediment size (Fig. 3B). The resulting map displays a band-like distribution with an approximate NE-SW orientation, showing an increase in grain size towards the NW (Fig. 3B). In general, it captures the variability of the data, especially in the northern sector where there is a higher density of samples.

In order to perform a detailed analysis, Folk (1954) sediment classification was used to re-categorize the samples. Since the sand-mud ratio is bellow 9:1, the classification of the samples is solely determined by the gravel percentage. The sampled points are grouped into 5 sedimentary types (Fig. 4A): Sand (% Gravel: 0–1); Slightly gravelly sand (1–5%); Gravelly sand (5–30%); Sandy Gravel, (30–80%) and Gravel (80–100%). The initial granulometric data and the new classification performed for each sample are available in Table 1. The samples exhibit a gravel content between 0–73% and thus, none of them are classified as gravel; 12 out of 28 samples correspond to gravelly sand, 7 are sand, 5 are sandy gravel and 4 are slightly gravelly sand. An ordinary kriging interpolation of the % Gravel was used to generate a Seabed Sediment Map (Fig. 4A): Four shades of blue are used to approximately depict the areas occupied by sediments, each corresponding to one of Folk´s (1954) granulometric categories. In the Seabed Sediment Map, more than half of the surveyed area is characterized by gravelly sands, accounting for 3.13 km^2 or 64.3% of the total area. Sandy gravels account for 9.8% (0.48 km^2) of the area, slightly gravelly sands for 14.2% (0.69 km^2), and sands for 11.7% (0.57 km^2). In comparison with previous studies that include the studied area (Galparsoro et al. 2010; Jouanneau et al. 2008), a more detailed map at a 1:10.000 scale is provided.

A thorough analysis of the Seabed Sediment Map reveals two main sectors separated by a small area identified as rocky substrate: the southern part, characterized by the presence of a paleochannel, and the region situated north of it. The majority of the sediment samples are located in the northern sector and, therefore, the obtained interpolation describes more reliably the granulometric distribution: a banded-shaped distribution with a NE-SW orientation, with sandy gravels to the NW and sands to the SE (Fig. 4B). This kind of distribution suggests a SE-directed flow, from the biggest sediment sizes to the smallest (Fig. 5A).

In the case of the paleochannel area, the interpolation also depicts a band-shaped distribution. However, it is influenced by the granulometric distribution of the northern area where most of the samples are located, and therefore it does not reflect the real pattern. There are 5 sediment samples available, concentrated in the southernmost part of the channel, that are not enough to generate an adequate interpolation. Moreover, one of the samples classified as slightly gravelly sand, shows gravel content just above the threshold required for classification as sand (SB04, % gravel: 1.35). Compared to the closest samples SB03 (% gravel: 0.18) and SB05 (% gravel: 0.27), the increased gravel content in sample SB04 could be influenced by erosion processes, as the sampling point is very close to the channel border. In contrast to the pattern observed in the northern area, in the paleochannel,

Table 1 Mean size and percentage of silt, sand and gravel of the 28 sediment samples

Sample	Sediment type		% Silt/Clay	%Sand	%Gravel	Mean size (μm)
SB01	Sandy gravel	sG	0.24	49.6	50.16	1474
SB02	Sand	S	0.02	99.68	0.3	504
SB03	Sand	S	0.23	99.59	0.18	316
SB04	Slightly gravelly sand	S	0.05	98.6	1.35	591
SB05	Sand	S	0.12	99.61	0.27	415
SB06	Sand	S	2.57	97.43	0	171
SB07	Sand	S	0	100	0	633
SB08	Sandy gravel	sG	0	26.37	73.63	2535
SB09	Gravelly sand	gS	0	94.04	5.96	665
SB010	Slightly gravelly sand	(g)S	0	95.32	4.68	819
SB011	Sand	S	0	99.15	0.85	588
SB012	Sandy gravel	sG	0	64.45	35.55	1595
SB013	Gravelly sand	gS	0.08	86.67	13.24	987
SB014	Gravelly sand	gS	0	85.28	14.72	1054
SB015	Slightly gravelly sand	(g)S	0	98.28	1.72	672
SB016	Gravelly sand	gS	0	91.33	8.67	1143
SB017	Gravelly sand	gS	0	80.21	19.79	1253
SB018	Sand	S	0	99.04	0.96	787
SB020	Gravelly sand	gS	0	83.73	16.27	1220
SB021	Slightly gravelly sand	(g)S	0	96.94	3.06	15.32
SB022	Gravelly sand	gS	0	84.42	15.32	1164
SB023	Gravelly sand	gS	0.26	81.28	18.72	1259
SB024	Gravelly sand	gS	0	91.69	8.31	1144
SB025	Sandy gravel	sG	0	62.77	36.16	1705
SB026	Gravelly sand	gS	1.08	92.57	7.43	1144
SB027	Sandy gravel	sG	0.6	55.82	43.58	1793
SB028	Gravelly sand	gS	0	94.57	5.43	1000
SB029	Gravelly sand	gS	0.07	75.06	24.87	1455

the sediment granulometric distribution is mainly influenced by river sediment supply, with the biggest sizes located in the south, close to the continent, and the smallest in the north, indicating sediment transport from south to north (Fig. 5A).

The aforementioned paleochannel is a 2 km long and 350 m wide (in its widest part) incised valley that reaches water depths of 59 m. As it represents the offshore extension of two present-day small rivers, we interpret it as a relict erosional feature formed during a period of relatively low sea level. The observed maximum depth of the channel could be related to the T8 terrace (65–67 m) defined by Bilbao-Lasa et al., (2020), generated between MIS (Marine Isotopic Stage) 5e and the Last Glacial Maximum. Since last glaciation around 17,000 years ago, sea level rose drowning the coastal area and filling river valleys with marine sediments until approximately 7000 years ago, when it is estimated that the sea level reached its present position at the Basque coast (Pascual et al. 2004). The transgression likely occurred rapidly, as evidenced by the preservation of the erosive feature of the channel, particularly in its southern portion. At the moment, it is filled with sediments with a probable mixed marine-fluvial origin (Fig. 4B). The geophysical survey report conducted by Esgemar (2017) for BIMEP describes a sediment fill in the channel with a thickness up to 7 m (Fig. 4B). The valley-fill deposits show a marked asymmetry in cross-section, with a gentle slope in the western side and a steep margin on the opposite side (Fig. 4B).

Morphodynamic analysis of bedforms

Bedforms elongated following an approximate N045 ºE axis are identified in two main sectors between 40 and 60 m depth. They exhibit spacing greater than 0.6 m and are thus classified as dunes (Flemming 2022 and references therein). However, based on their size, they can be divided into two groups (Fig. 5): one situated in the southwestern area (Fig. 5B) and the other in the southeastern area (Fig. 5C). Bedforms from the southwestern part vary in size, ranging from a minimum length of 55 m to a maximum extent of 700 m, but are in general larger than the ones in the SE. They display heights between 1.2 and 1.7 m and are irregularly

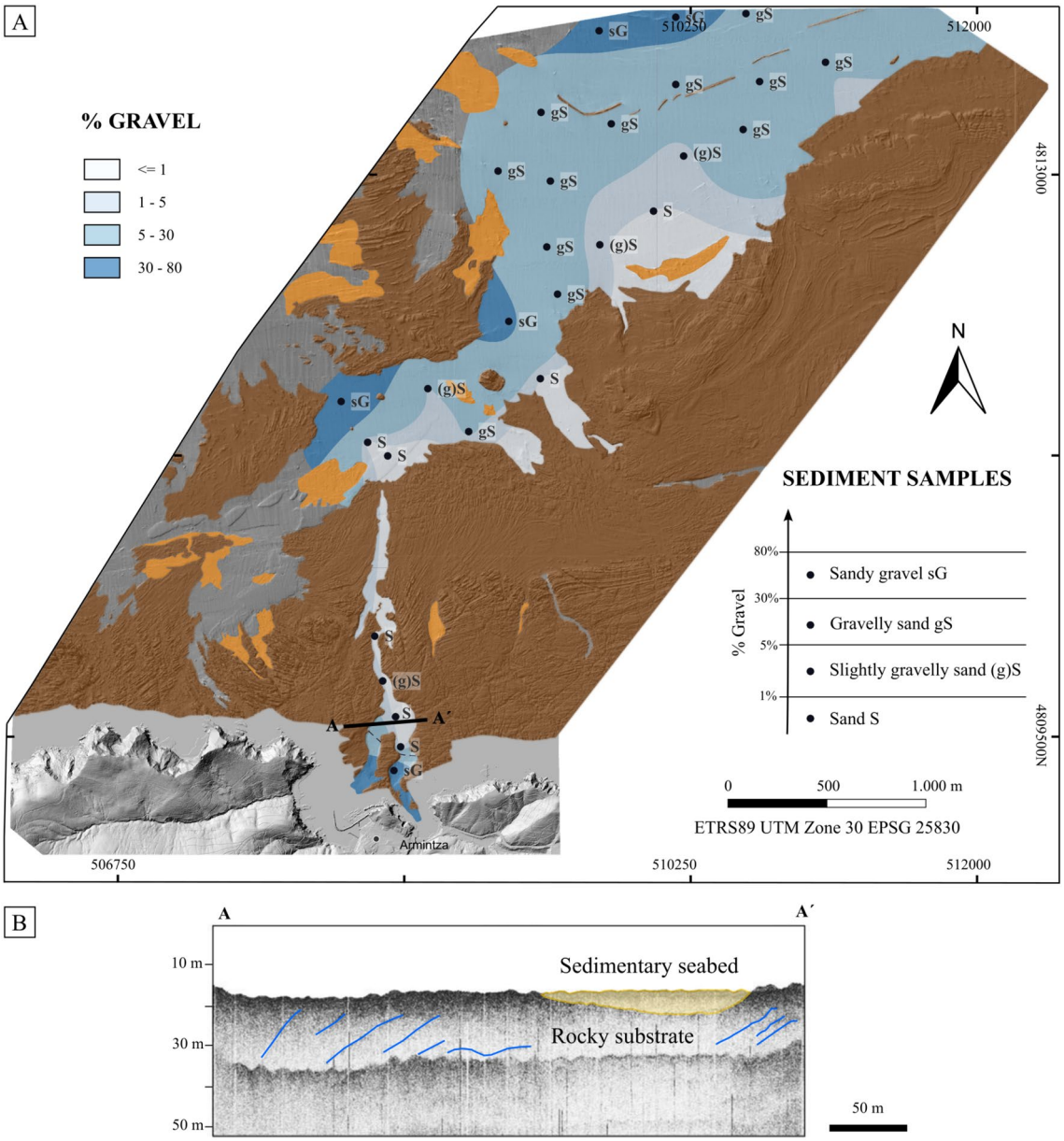

Fig. 4 **a** Seabed sediment map categorized by % gravel content. Folk (1954) sediment classification is used to establish the boundaries between categories. Abbreviations representing the corresponding category are included next to each sediment sample; **b** Seismic line across the paleochannel (see Fig. 4A for location), modified from Esgemar (2017). The erosion of the paleochannel into the rocky substrate and its filling with unconsolidated sediments is shown. The blue lines indicate bedding planes in the rocky substrate

spaced, with distances between 20 and 100 m. They are slightly irregularly shaped, asymmetric, with a stoss side oriented towards the NW and a lee side towards the SE, and a relatively flat surface (Fig. 5D). In the southeastern area smaller bedforms with lengths ranging from 10 to 90 m are observed; they display sizes close to the bathymetry resolution limit, but an average approximate height lower of 0.5 m and spacing close to 3 m are estimated.

Assuming that these bedforms are formed due to the interaction between bathymetry and flow, the direction of the prevailing current would be predominantly unidirectional and perpendicular to the elongation of the forms. Within the study area, the N045 ºE orientation of the bedforms suggests a NW–SE oriented current, with a mean orientation N135 ºE (Fig. 5). Due to the relatively small size of the bedforms in the SE, it is challenging to conduct an asymmetry analysis to precise the sense of the flow. However, in the case of the ones in the SW, the inclination of the stoss side towards the NW (Fig. 5D) suggests a SE-directed flow, which aligns with the flow influencing the previously described granulometric

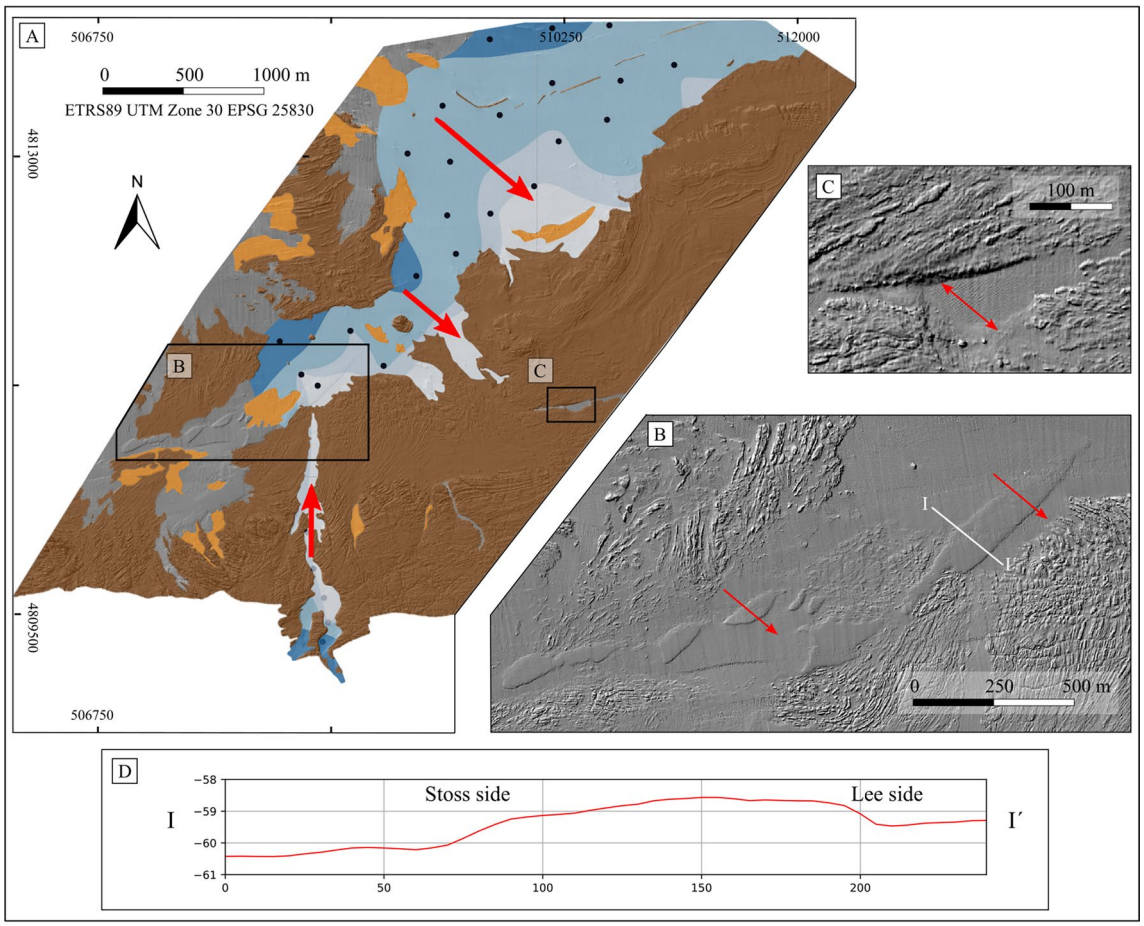

Fig. 5 Integration of sediment mobility data: **a** Seabed sediment map with the sediment movement direction (red arrows); **b** and **c** Detailed views of the identified bedforms (see Fig. 5A for location). The red arrows indicate the flow direction deduced from their asymmetry. In the case of Fig. 5C, the size of the bedforms close to the resolution limit doesn´t allow the definition of the flow sense, only its direction; **d** Bathymetric profile of one of the bottom features classified as dunes (location in Fig. 5B), illustrating the stoss side (NW) and the lee side (SE)

distribution. This observation supports the presence of a consistent SE-directed current that affects both bedform generation and sediment distribution.

According to their origin, sand waves are classified into relict bedforms, formed during the Last Glacial Maximum in shallow coastal waters and submerged to their current depth after the Holocene sea level rise, and active features, which are still forming, changing and evolving in equilibrium with current hydrodynamic conditions (Albarracín et al. 2014; Luan et al. 2010; Yang et al. 2022). Given the varying depths of the study area and the progressive nature of the sea level rise, characterized by periods of rapid elevation followed by more stable phases, different parts of the area would have submerged at different times, allowing for the development of relict bedforms in shallow marine environments, which were later modified or preserved as the sea continued to rise.

On the Basque shelf, previous studies identified an E-W oriented wind-generated surface current responsible for fine sediment and pollutant migration patterns (Chiri et al. 2019; González et al. 2006; Ibañez 1979; Uriarte et al. 2004), which does not correspond with the deduced SE-directed current orientation. However, the proposed SE current direction matches the primary incoming wave direction from the NW, including the most energetic waves and the swell associated with large storms from the North-Atlantic (Galparsoro et al. 2012; Ibarra-Berastegi et al. 2018). The presence of both bedforms and granulometric sediment distribution at depths greater than the storm wave base on the Basque shelf, established between −30 and −35 m (Galparsoro et al. 2010), suggests that the SE-directed current governing sediment transport in BIMEP is generated by swells associated with large storms. This interpretation is consistent with previous studies near the area (Galparsoro et al. 2010) and in the French continental shelf of the Bay of Biscay, which verified that below 10 m depth the repetition of storm-related energetic events can explain mayor

sand mobilization (Barthe and Castaing 1989; Castaing 1981; OSPAR Commission 2000). Thus, the current oceanographic conditions correspond well with the observed bedform morphology and granulometric distribution pattern of the sediment. Nevertheless, complementary data, such as time-series and bottom current measurements, are needed to precisely determine the origin of the bedforms and whether the related SE-directed bottom current is pre-Holocene or is still active.

Conclusions

This work outlines a methodological example for conducting a preliminary geological characterization of offshore renewable energy sites using pre-existing information acquired for other purposes. A litho-structural analysis of the coastal zone and continental shelf of BIMEP allows for the prediction of lithology and the approximate bedding orientation in the study area. Fracture analysis determines that the primary fractures are oriented NE-SW and NW–SE. Additionally, a precise characterization of sediment-covered areas and rocky bottoms is provided through a detailed seafloor type map, crucial for a preliminary determination of mooring and foundation types for offshore wind installations, as it directly relates to the seabed type.

Furthermore, a detailed examination of sediment-covered areas suggests the presence of a SE-directed bottom current, likely related to storm-induced waves. This current may mobilize sediment, leading to granulometric classification and the creation of NE-SW oriented bedforms. Although time-series data and complementary studies are necessary, this direction aligns with the current orientation generated by extreme storm events, suggesting that the bedforms are active features. Identifying these sediment transport patterns offers valuable insights for understanding sediment dynamics and managing offshore infrastructure accordingly. This comprehensive analysis significantly enhances regional knowledge of the seafloor, providing essential insights for optimizing future geophysical and geotechnical campaigns and reducing costs. Moreover, this data could help quantify the foundation impact on the seafloor, helping to predict and mitigate potential affections, such as scour or wake effects.

Overall, the integration of this study's findings with existing geological and oceanographic knowledge not only enhances the understanding of sediment dynamics and structural geology but also supports more informed decision-making for future offshore renewable energy projects. The results underscore the importance of continued research and monitoring to adapt to evolving environmental conditions and technological advancements.

Acknowledgements We would like to thank BIMEP for provided data. Open Access funding is provided by University of the Basque Country. This work was supported by project PID2022-136948NB-100/AEI/https://doi.org/10.13039/501100011033/FEDER, UE (Spanish Ministry of Science and Innovation), project GIU23/003 (University of the Basque Country, UPV/EHU), project EUSK22/05 (Euskampus Fundazioa) and project EUSK22/09 (Euskampus Fundazioa).

Author contributions Iván Asensio –conducted the investigation, mapping and data acquisition, fieldwork, methods, analysis and interpretation of results, elaborated figures, writing. Lidia Rodríguez-Méndez – conceptualization, conducted the investigation, analysis and interpretation of results, elaborated figures, writing, review, supervision. Néstor Vegas – conceptualization, analysis and interpretation of results, elaborated figures, writing, review, supervision. Aitor Aranguren – analysis and interpretation of the results, review.

Funding Open Access funding provided thanks to the CRUE-CSIC agreement with Springer Nature. This work was supported by project PID2022-136948NB-100/AEI/https://doi.org/10.13039/501100011033/FEDER, UE (Spanish Ministry of Science and Innovation), project GIU23/003 (University of the Basque Country, UPV/EHU), project EUSK22/05 (Euskampus Fundazioa) and project EUSK22/09 (Euskampus Fundazioa).

Data availability No datasets were generated or analysed during the current study.

Declarations

Conflict of interest The authors declare no competing interests.

References

Ábalos B (2016) Geologic map of the basque-cantabrian basin and a new tectonic interpretation of the Basque Arc. Int J Earth Sci 105:2327–2354. https://doi.org/10.1007/s00531-016-1291-6

Ábalos B, Elorza J (2012) Structural diagenesis of siderite layers in black shales (Albian Black Flysch, Northern Spain). J Geol 120:405–429. https://doi.org/10.1086/665794

Agirrezabala LM, Sarrionandia F, Carracedo-Sánchez M (2017) Diatreme-forming volcanism in a deep-water faulted basin margin: lower cretaceous outcrops from the basque-cantabrian basin, western pyrenees. J Volcanol Geoth Res 337:124–139. https://doi.org/10.1016/j.jvolgeores.2017.03.019

Agirrezabala LM, Malaxetxebarria A, Pascual A, Rodríguez-Lázaro J (2023) Deep-sea paleoenvironmental evolution in the mid-Cretaceous of the Basque Pyrenees based on microfaunal analysis

(Armintza section). Cont Shelf Res 260:105001. https://doi.org/10.1016/j.csr.2023.105001
Albarracín S, Alcántara-Carrió J, Montoya-Montes I, Fontán-Bouzas Á, Somoza L, Amos CL, Salgado JR (2014) Relict sand waves in the continental shelf of the Gulf of Valencia (Western Mediterranean). J Sea Res 93:33–46. https://doi.org/10.1016/j.seares.2013.12.014
Amjadian P, Neill SP, Martí Barclay V (2023) Characterizing seabed sediments at contrasting offshore renewable energy sites. Front Marine Sci. https://doi.org/10.3389/fmars.2023.1156486
Asensio I, Rodríguez-Méndez L, Vegas N, Aranguren A (2024) Geological study of the seafloor applied to marine renewable energies. J Maps 20:2422543. https://doi.org/10.1080/17445647.2024.2422543
Bald J (2017) Estudio Batimétrico en BIMEP. Informe para BIMEP, S.A.:9
Barthe X, Castaing P (1989) Étude théorique de l'action des courants de marée et des houles sur les sédiments du plateau continental du Golfe de Gascogne. Oceanologica Acta (in French with English Abstract) 12:325–334
Bilbao-Lasa P, Jara-Muñoz J, Pedoja K, Alvarez I, Aranburu A, Iriarte E, Galparsoro I (2020) Submerged marine terraces identification and an approach for numerical modeling the sequence formation in the bay of biscay (Northeastern Iberian Peninsula). Front Earth Sci 8:1. https://doi.org/10.3389/feart.2020.00047
Cai L, Hu Q, Qiu Z, Yin J, Zhang Y, Zhang X (2023) Study on the impact of offshore wind farms on surrounding water environment in the yangtze estuary based on remote sensing. Remote Sens 15:5347
Castaing P (1981) Le transfert à l'océan des suspensions estuariennes: cas de la Gironde. Université de Bordeaux I
Castañares LM, Robles S, Gimeno D, Vicente Bravo JC (2001) The submarine volcanic system of the errigoiti formation (Albian-Santonian of the Basque-Cantabrian Basin, Northern Spain): stratigraphic framework, facies, and sequences. J Sediment Res 71:318–333. https://doi.org/10.1306/080700710318
Chiri H, Cid A, Abascal AJ, García-Alba J, García A, Iturrioz A (2019) A high-resolution hindcast of sea level and 3D currents for marine renewable energy applications: A case study in the Bay of Biscay. Renew Energy 134:783–795. https://doi.org/10.1016/j.renene.2018.11.069
Clark S, Schroeder F, Baschek B (2014) The influence of large offshore wind farms on the North Sea and Baltic Sea. A comprehensive literature review. p 35
Commission OSPAR (2000) Quality Status Report 2000: Region IV – Bay of Biscay and Iberian Coast. The Commission, London, p 134
DeFelipe I, Pulgar JA, Pedreira D (2018) Crustal structure of the eastern basque-cantabrian zone – western pyrenees: from the cretaceous hyperextension to the cenozoic inversion. Revista De La Sociedad Geologica De Espana 31:69–82
Ercilla G, Casas D, Estrada F, Vázquez JT, Iglesias J, García M, Gómez M, Acosta J, Gallart J, Maestro-González A (2008) Morphosedimentary features and recent depositional architectural model of the Cantabrian continental margin. Mar Geol 247:61–83. https://doi.org/10.1016/j.margeo.2007.08.007
ESGEMAR (2017) Campaña de sísmica de reflexión en el área de BIMEP, Armintza (Vizcaya). Informe de resultados para Biscay Marine Energy Platform S.A.:31.
Ferrer L, Fontán A, Mader J, Chust G, González M, Valencia V, Uriarte A, Collins MB (2009) Low-salinity plumes in the oceanic region of the basque country. Cont Shelf Res 29:970–984. https://doi.org/10.1016/j.csr.2008.12.014
Flemming B (2022) The limits to growth: how large can subaqueous, flow-transverse bedforms ultimately become? Ocean Dyn 72:801–815. https://doi.org/10.1007/s10236-022-01527-7
Folk RL (1954) The distinction between grain size and mineral composition in sedimentary-rock nomenclature. J Geol 62:344–356. https://doi.org/10.1086/626171
Fontán A, Cornuelle B (2015) Anisotropic response of surface circulation to wind forcing, as inferred from high-frequency radar currents in the southeastern Bay of Biscay. J Geophys Res: Oceans. https://doi.org/10.1002/2014JC010671
Fontán A, Mader J, González M, Uriarte A, Gyssels P, Collins MB (2006) Marine hydrodynamics between San Sebastián and Hondarribia (Guipúzcoa, northern Spain): Field measurements and numerical modelling. Sci Mar 70:51–63. https://doi.org/10.3989/scimar.2006.70s151
Fontán A, González M, Wells N, Collins M, Mader J, Ferrer L, Esnaola G, Uriarte A (2009) Tidal and wind-induced circulation within the southeastern limit of the Bay of Biscay: Pasaia Bay, Basque Coast. Cont Shelf Res 29:998–1007. https://doi.org/10.1016/j.csr.2008.12.013
Galparsoro I, Borja A, Legorburu I, Hernández C, Chust G, Liria P, Uriarte A (2010) Morphological characteristics of the Basque continental shelf (Bay of Biscay, northern Spain); their implications for Integrated Coastal Zone Management. Geomorphology 26:314–329. https://doi.org/10.1016/j.geomorph.2010.01.012
Galparsoro I, Liria P, Legorburu I, Bald J, Chust G, Ruiz-Minguela P, Pérez G, Marqués J, Torre-Enciso Y, González M, Borja Á (2012) A marine spatial planning approach to select suitable areas for installing wave energy converters (wecs), on the basque continental shelf (Bay of Biscay). Coast Manag 40:1–19. https://doi.org/10.1080/08920753.2011.637483
Galparsoro I, Menchaca I, Seeger I, Nurmi M, McDonald H, Garmendia JM, Pouso S, Borja Á (2022) Mapping potential environmental impacts of offshore renewable energy. ETC/ICM Report 2/2022: European Topic Centre on Inland, Coastal Marine Waters. 2:123
Garrote Ruiz A, García Portero J, Muñoz Jiménez L, Arriola Garrido A, Eguiguren Altuna E, García Pascual I, Garrote Ruiz R (1987) Memoria y mapa geológico a escala 1:25.000 de la hoja nº 37 (Armintza). In: Energía EVdl (ed),
Gómez M, Vergés J, Riaza C (2002) Inversion tectonics of the northern margin of the Basque Cantabrian Basin. Bulletin De La Société Géologique De France 173:449–459. https://doi.org/10.2113/173.5.449
González M, Uriarte A, Fontán A, Mader J, Gyssels P (2004) Chapter 6 - Marine Dynamics. In: Borja Á, Collins M (eds) Elsevier Oceanography Series. Elsevier, pp 133–157
González M, Uriarte A, Pozo R, Collins M (2006) The prestige crisis: operational oceanography applied to oil recovery, by the basque fishing fleet. Mar Pollut Bull 53:369–374. https://doi.org/10.1016/j.marpolbul.2005.02.046
Ibañez M (1979) Hydrological studies and surface currents in the coastal area of the Bay of Biscay. Lurralde 2:37–75
Ibarra-Berastegi G, Sáenz J, Ulazia A, Serras P, Esnaola G, Garcia-Soto C (2018) Electricity production, capacity factor, and plant efficiency index at the Mutriku wave farm (2014–2016). Ocean Eng 147:20–29. https://doi.org/10.1016/j.oceaneng.2017.10.018
Iglesias G, Carballo R (2010) Wave energy and nearshore hot spots: The case of the SE Bay of Biscay. Renewable Energy 35:2490–2500. https://doi.org/10.1016/j.renene.2010.03.016
Irabien MJ, Cearreta A, Gómez-Arozamena J, Gardoki J, Martín-Consuegra AF (2020) Recent coastal anthropogenic impact recorded in the Basque mud patch (southern Bay of Biscay shelf). Quatern Int 566–567:357–367. https://doi.org/10.1016/j.quaint.2020.03.042
Jiang Z (2021) Installation of offshore wind turbines: A technical review. Renew Sustain Energy Rev 139:110576. https://doi.org/10.1016/j.rser.2020.110576

Jouanneau JM, Weber O, Champilou N, Cirac P, Muxika I, Borja A, Pascual A, Rodríguez-Lázaro J, Donard O (2008) Recent sedimentary study of the shelf of the Basque country. J Mar Syst 72:397–406. https://doi.org/10.1016/j.jmarsys.2007.03.013

Lagabrielle Y, Bodinier J-L (2008) Submarine reworking of exhumed subcontinental mantle rocks: field evidence from the Lherz peridotites, French Pyrenees. Terr Nova 20:11–21. https://doi.org/10.1111/j.1365-3121.2007.00781.x

Lamolda MA, Orue-Etxebarria X, Proto-Decima F (1983) The cretaceous-tertiary boundary in sopelana (Biscay, Basque Country). Zitteliana 10:663–670

Lopez-Horgue MA, Owen HG, Aranburu A, Fernandez-Mendiola PA, Garcia-Mondéjar J (2009) Early late Albian (Cretaceous) of the central region of the Basque-Cantabrian Basin, northern Spain: biostratigraphy based on ammonites and orbitolinids. Cretac Res 30:385–400. https://doi.org/10.1016/j.cretres.2008.08.001

López-Horgue MA, Owen HG (2024) Mortoniceratinae (Ammonoidea) from the lower upper Albian of the Basque-Cantabrian basin (Western Pyrenees): New records, new taxa and their taxonomic and biostratigraphical value. Cretac Res 158:105855. https://doi.org/10.1016/j.cretres.2024.105855

Luan X, Peng X, Wang Y, Qiu Y (2010) Activity and formation of sand waves on northern South China Sea shelf. Journal of Earth Science 21:55–70. https://doi.org/10.1007/s12583-010-0005-4

Net-Zero-Industry-Act (2023) Regulation of the European Parliament and of the Council on establishing a framework of measures for strenghtening Europe´s net-zero technology products manufacturing ecosystem. European Commission. In: Union E (ed), Document 52023PC0161

Net-Zero-Tracker (2023) Net Zero Stocktake 2023: New Climate Institute, Oxford Net Zero, Energy and Climate Intelligence Unit and Data-Driven EnviroLab. In: Institute; N, Zero; ON, Unit; EaCI, EnviroLab; D-D (eds), Net Zero Tracker,

Nyberg B, Nixon CW, Sanderson DJ (2018) NetworkGT: A GIS tool for geometric and topological analysis of two-dimensional fracture networks. Geosphere 14:1618–1634. https://doi.org/10.1130/ges01595.1

Pascual A, Cearreta A, Rodriguez-Lazaro J, Uriarte A (2004) Chapter 3 Geology and Palaeoceanography. Elsevier, NY, pp 53–73

Pedreira D, Pulgar JA, Gallart J, Torné M (2007) Three-dimensional gravity and magnetic modeling of crustal indentation and wedging in the western pyrenees-cantabrian mountains. J Geophys Res: Solid Earth. https://doi.org/10.1029/2007JB005021

Pedrera A, García-Senz J, Peropadre C, Robador A, López-Mir B, Díaz-Alvarado J, Rodríguez-Fernández LR (2021) The Getxo crustal-scale cross-section: testing tectonic models in the Bay of Biscay-Pyrenean rift system. Earth Sci Rev 212:103429. https://doi.org/10.1016/j.earscirev.2020.103429

Petrie Hannah E, Eide Christian H, Haflidason H, Watton T (2022) A conceptual geological model for offshore wind sites in former ice stream settings: the Utsira Nord site, North Sea. J Geol Soc. https://doi.org/10.1144/jgs2021-163

Poprawski Y, Basile C, Agirrezabala LM, Jaillard E, Gaudin M, Jacquin T (2014) Sedimentary and structural record of the Albian growth of the Bakio salt diapir (the Basque Country, northern Spain). Basin Res 26:746–766. https://doi.org/10.1111/bre.12062

Puelles P, Ábalos B, García de Madinabeitia S, Sánchez-Lorda ME, Fernández-Armas S, Gil Ibarguchi JI (2014) Provenance of quartz-rich metamorphic tectonite pebbles from the "Black Flysch" (W Pyrenees, N Spain): An EBSD and detrital zircon LA–ICP-MS study. Tectonophysics 632:123–137. https://doi.org/10.1016/j.tecto.2014.06.004

Puelles P, Agirrezabala LM, Sarrionandia F, Ábalos B, Carracedo-Sánchez M, Gil-Ibarguchi JI (2017) Discerning Permian orogenic metamorphism from other tectonothermal events (Mesoproterozoic to Alpine, contact to orogenic or extensional) in the concealed basement of the Basque-Cantabrian Basin (northern Spain). Lithosphere 9:441–452. https://doi.org/10.1130/l619.1

Pujalte V, Robles S, García Mondéjar J (1986) Características sedimentológicas y paleogeográficas del fan-delta albiense de la Formación Monte Grande y sus relaciones con el flysch Negro (Arminza-Górliz, Vizcaya). Acta Geológica Hispánica 21:141–150

Quero García P, Chica Ruiz JA, García Sanabria J (2020) Blue energy and marine spatial planning in Southern Europe. Energy Policy 140:111421. https://doi.org/10.1016/j.enpol.2020.111421

Rat P, Feuillée P (1967) Structures et paléogéographies Pyrénéo - Cantabriques. Institut des Sciences de la Terre Université e Dijon VI:1–48.

Robles S, Pujalte V, García-Mondéjar J (1988) Evolución de los sistemas sedimentarios del Margen continental Cantábrico durante el Albiense y Cenomaniense, en la transversal del litoral vizcaíno. Revista De La Sociedad Geologica De Espana (in Spanish with English Abstract) 1:409–441

ROBOTIKER (2009) Sedimentology study for the EIA (bimep: Biscay Marine Energy Platform). Tecnalia, Corporación Tecnológica. p 40

Roca E, Ferrer O, Rowan MG, Muñoz JA, Butillé M, Giles KA, Arbués P, de Matteis M (2021) Salt tectonics and controls on halokinetic-sequence development of an exposed deepwater diapir: The Bakio Diapir, Basque-Cantabrian Basin. Pyrenees Marine and Petroleum Geology 123:104770. https://doi.org/10.1016/j.marpetgeo.2020.104770

Rodríguez-Méndez L, Vegas N, Aranguren A (2022) Aplicación de datos batimétricos en la cartografía geológica de la plataforma continental. Un ejemplo de la costa occidental del País Vasco. Libro Resúmenes X Simposio sobre el Margen Ibérico Atlántico (MIA). p 106

Tugend J, Manatschal G, Kusznir NJ, Masini E, Mohn G, Thinon I (2014) Formation and deformation of hyperextended rift systems: Insights from rift domain mapping in the Bay of Biscay-Pyrenees. Tectonics 33:1239–1276. https://doi.org/10.1002/2014TC003529

Ubide T, Wijbrans JR, Galé C, Arranz E, Lago M, Larrea P (2014) Age of the Cretaceous alkaline magmatism in northeast Iberia: Implications for the Alpine cycle in the Pyrenees. Tectonics 33:1444–1460. https://doi.org/10.1002/2013TC003511

United-Nations (2015) Paris agreement to the United Nations Framework Convention on Climate Change (UNFCC). Transform Our World: the Agenda Sustain Develop 1:49

Uriarte A (1998) Sediment dynamics on the inner continental shelf of the Basque Country (NSpain). University of Southampton

Uriarte A, Collins M, Cearreta A, Bald J, Evans G (2004) Sediment supply, transport and deposition: contemporary and Late Quaternary evolution. In: Borja Á, Collins M (eds) Oceanography and Marine Environment of the Basque Country. Elsevier Oceanography series, NY, pp 97–132

Vázquez R, Cabos W, Nieto-Borge JC, Gutiérrez C (2024) Complementarity of offshore energy resources on the Spanish coasts: Wind, wave, and photovoltaic energy. Renewable Energy 224:120213. https://doi.org/10.1016/j.renene.2024.120213

Velenturf APM, Emery AR, Hodgson DM, Barlow NLM, Mohtaj Khorasani AM, Van Alstine J, Peterson EL, Piazolo S, Thorp M (2021) Geoscience solutions for sustainable offshore wind development. Earth Sci, Syst Soc. https://doi.org/10.3389/esss.2021.10042

Wang T, Ru X, Deng B, Zhang C, Wang X, Yang B, Zhang L (2023) Evidence that offshore wind farms might affect marine sediment quality and microbial communities. Sci Total Environ 856:158782. https://doi.org/10.1016/j.scitotenv.2022.158782

Wentworth CK (1922) A scale of grade and class terms for clastic sediments. J Geol 30:377–392. https://doi.org/10.1086/622910

Yang Y, Liu M, Xu J, Xu W (2022) Migrating sandwaves riding on relict dunes of Taiwan shoal, northern South China Sea. Front Earth Sci. https://doi.org/10.3389/feart.2022.975220